Constitutive Modelling of Skin Growth

Adrian Buganza Tepole and Arun K. Gosain

Abstract Skin, like all biological materials, adapts to mechanical cues. When expanded beyond its physiological regime over extended time periods, skin grows. This intuitive knowledge has been leveraged clinically in a widely used surgical technique called tissue expansion, in which a surgeon inserts a balloon-like device and inflates it gradually over months to grow skin for reconstructive purposes. However, it is currently not possible to anticipate how much of the deformation due to the expander is growth and how much of it is elastic strain, and tissue expansion protocols remain arbitrary, based on each physician's experience and training, leading to an unacceptable frequency of complications. Here we show a continuum mechanics framework to describe skin growth based on the multiplicative split of the deformation gradient in to growth and elastic tensors. We present the corresponding finite element implementation, in which the growth component is an internal variable stored and updated at the integration points of the finite element mesh. The model is applied to study the deformation and growth patterns of skin for different expander shapes, as well as in patient specific scenarios, showing excellent qualitative agreement with clinical experience. Experimental methods to calibrate and validate the translation of the model to the clinical setting are briefly discussed. We expect that the proposed modeling framework will increase our fundamental understanding of how skin grows in response to stretch, and it will soon lead to personalized treatment plans to achieve the desired patterns of skin growth while minimizing complications.

A. B. Tepole (✉)
School of Mechanical Engineering and Weldon School of Biomedical Engineering, Purdue University, West Lafayette, IN, USA
e-mail: abuganza@purdue.edu

A. K. Gosain
Feinberg School of Medicine, Northwestern University, Chicago, IL, USA

G. Limbert (ed.), *Skin Biophysics*, Studies in Mechanobiology, Tissue Engineering and Biomaterials 22,
https://doi.org/10.1007/978-3-030-13279-8_3

1 Introduction

Unlike structural materials, living tissues have the capacity to adapt to the environment, and in particular to mechanical cues. There are two main mechanisms by which tissues respond chronically to mechanical input: growth and remodeling. Growth is the addition of mass, and remodeling is associated to permanent changes in microstructure [1]. Skin growth is encountered in our everyday lives; we all probably have noticed changes in skin surface area when we gain or lose weight. Pregnancy also induces remarkable and evident skin adaptation, both growth and remodeling [2]. Yet, this intuitive notion about our everyday tissue adaptation had not captivated our scientific interest or the ambition to systematically control skin growth for medical applications until recently.

The first reported case of tissue expansion dates to 1957 when Dr. Neumann implanted a balloon in the neck of a patient who had lost an ear. He then inflated the balloon with water over a period of 8 weeks. When the balloon was taken out, skin had grown approximately 50% with respect to the initial area of skin, and the new tissue was used to reconstruct the ear [3]. This was the first example of tissue expansion, a technique that has since revolutionized reconstructive surgery [4–6]. At the core of tissue expansion is the ability to leverage the remarkable adaptation of skin growth in response to stretch beyond the physiological limit for the creation of skin flaps.

Currently, tissue expansion is used ubiquitously in the field of plastic and reconstructive surgery, to resurface large portions of skin after removal of giant birth defects (termed nevus), to reconstruct breasts after mastectomy, to create new skin for burn patients, and to grow skin needed after the excision of skin cancer [7, 8]. Tissue expanders are produced by different manufactures and they come in different sizes and shapes. The popularity of this procedure hinges on its crucial capacity to grow new tissue that has the same mechanical properties, appearance, and blood supply as the surrounding skin, making it particularly ideal for aesthetic reasons [9]. Yet, despite the demand for this procedure, there are still no tools to predict how skin adapts to stretch, and the current treatment planning continues to rely extensively on the surgeon's experience and training rather than on engineering design tools. Unfortunately, complications and suboptimal outcomes are still common and there is no gold standard for the treatment strategy of individual patients. Instead, there are many arbitrary tissue expansion protocols [10–12].

In this chapter we show the latest progress in modeling skin growth in response to stretch beyond the physiological regime, how simulations of skin growth can be used to increase our fundamental understanding of tissue adaptation, and as a stepping stone towards the incorporation of computational tools in routine clinical practice with the end goal of aiding in the decision making process and minimizing complications from tissue expansion.

Figure 1 shows the case of an 11-year old who had a giant nevus in the right shoulder that was to be resected. Nevi are giant birthmarks associated with increased

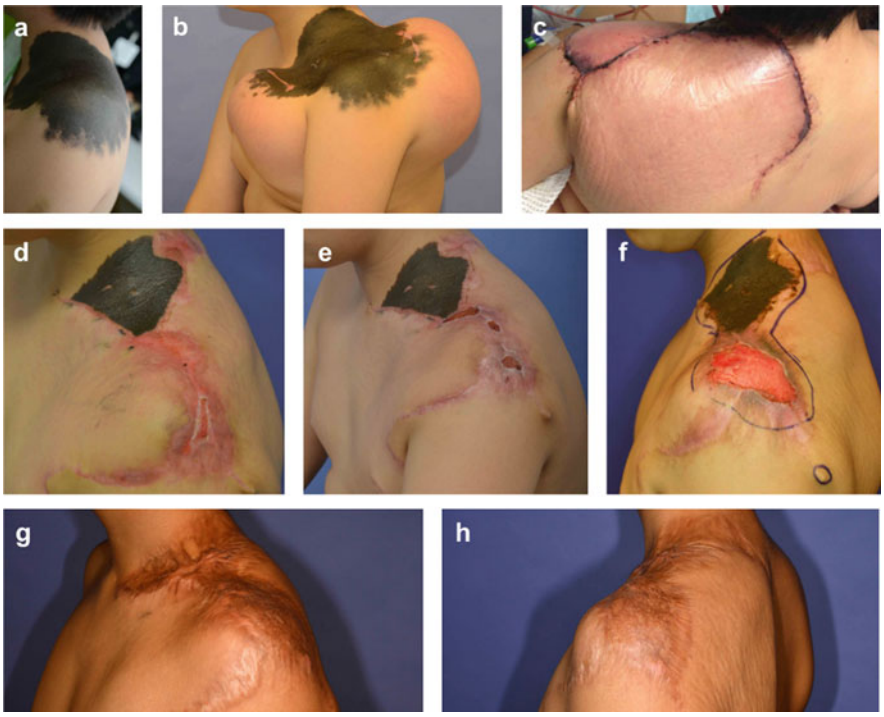

Fig. 1 Complications after tissue expansion. (**a**) 11-year-old patient with giant nevus. (**b**) Tissue expanders were used to grow skin by chronic overstretch. (**c**) Expanded tissue was advanced to correct the defect. (**d–f**) Excessive tension due to insufficient skin growth led to a chronic wound. (**g–h**) After full thickness graft there was scarring and contracture at the neck and shoulder

risk of malignancy and constitute a concern for psychological development during childhood and are hence typically resected early in life [13]. In the case shown, two tissue expanders were placed and gradually inflated over several months. At the end of the inflation, the expanders were removed and the newly grown skin was used to reconstruct the adjacent area. Unfortunately, the amount of grown skin was less than needed and the resulting flaps were closed under significant tension, leading to wound dehiscence and necrosis. Ultimately, a full thickness graft was needed, but the secondary intention healing concluded in a hypertrophic scar with contracture. Had there been tools to predict and monitor the amount of newly grown skin and the resulting flap deformation, this patient would have received an uneventful treatment plan without complications.

Schematically, the underlying biological control of skin adaptation is shown in Fig. 2. In vivo, the skin is in a homeostatic configuration, possibly with some residual stress [14]. The tissue expanders, gradually inflated over a long time period, impose supra-physiological deformations that trigger local adaptation, i.e. growth. As a result, homeostasis is regained locally. When the expander is removed, the

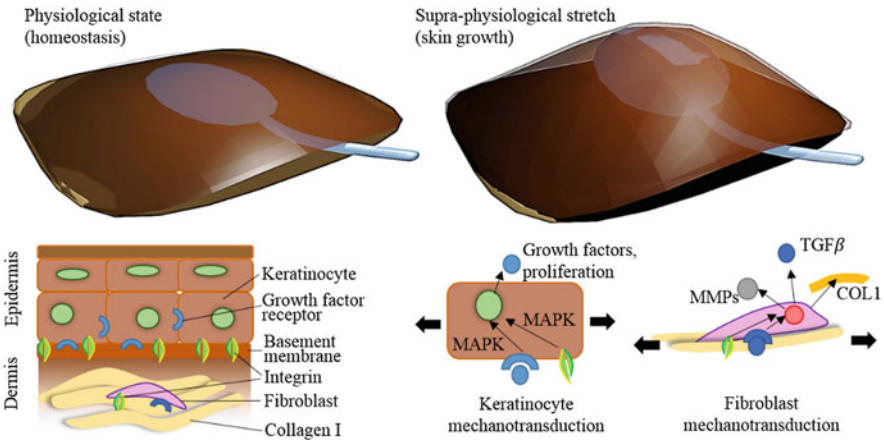

Fig. 2 Skin mechanotransduction. In the physiological state the skin is in local homeostasis. There are two main cell types present in skin, keratinocytes in the epidermis and fibroblast in the dermis. These cells response to mechanical cues and modify their immediate environment to regain homeostasis, leading to skin growth

grown skin is used for reconstructive purposes [15]. From the surgeon's point of view, the primary challenge in anticipating the amount of new skin comes from the fact that the observed deformation is a combination of prestrain, elastic deformation, and growth [16]. The continuum mechanics framework for finite volumetric growth presented here is an ideal approach to model the interplay between the different components of the deformation.

While it is evident that skin grows in response to stretch, the underlying biological mechanisms remain poorly understood. Figure 2 shows our current understanding of the biological pathways involved in skin mechanoadaptation. As for all living matter, the cells resident in the tissue are the ones responsible for sensing the local stress or deformation, transforming these mechanical inputs into chemical signals, and responding in consequence by altering their proliferation rate and remodeling their extra cellular matrix (ECM). The process by which cells interpret stress and strain, turning them into chemical signals inside the cell, is called mechanotransduction [17]. We emphasize the notion of a local homeostatic configuration determined by a single cell in their immediate micro-environment. In other words, as illustrated in Fig. 2, skin growth can be modeled as a local process determined by the cell response. This assumption aligns well with experimental evidence showing that growth is greater in zones of higher deformation [16].

The skin is made out of two layers, the epidermis is at the top and the dermis is at the bottom [18]. Keratinocytes are the most abundant cell population in the epidermis, while the main resident cells of the dermis are the fibroblasts. At the interface between dermis and epidermis there is a basement membrane made out of collagen type IV and laminin that serves as an anchoring matrix for the first layer of keratinocytes [19]. This initial layer of the epidermis is also called the basal

layer. Basal keratinocytes are tasked with the constant renewal of the epidermis [20]. When a basal keratinocyte divides asymmetrically creating a daughter cell that is not in contact with the basement membrane, this cell continues a process of terminal differentiation as it makes its way to the outer surface where it is released by desquamation [21]. Other layers of the epidermis are thus non proliferative. Not surprisingly, basal keratinocytes are the most important mechanosensitive cells in the epidermis [22]. Mechanosensing by these cells is associated primarily with integrin signaling [23]. Integrins are proteins that serve as anchoring points between the cell membrane and the surrounding ECM, and have been recognized as a general mechanosensing tool across cell types [24]. In the epidermis, integrins concentrate in the basal layer [25]. In the rest of the epidermis, cell-cell adhesion is regulated by desmosomes [26]. There are also indirect mechanotransduction pathways. For instance, integrin signaling has been shown to crosstalk with growth factor receptors such as epithelial growth factor receptor (EGF-R) [23, 27]. Both of these pathways ultimately leads to increase keratinocyte proliferation through mitogen-activated protein (MAP) kinase signaling [28].

In the dermis, fibroblasts are a hallmark example of mechanosensitive cells [29]. The dermis is primarily made out of collagen type I, and fibroblasts constitute a scarce cell population in this environment [30]. Fibroblasts sense mechanical signals through integrins which serve as their attachment points to the ECM. Upon stretch, integrin signaling is linked to three crucial cell processes needed for ECM remodeling. First, fibroblasts collagen remodeling is widely regulated by the transforming growth factor beta (TGF-β) signaling pathway. In response to applied stretch, TGF-β1 is upregulated [31]. Activation of this pathway then contributes to the regulation of the collagen network. Collagen production is the second process of interest. For skin growth, new ECM must be created, which entails production of collagen by fibroblasts. In response to stretch, fibroblasts show increased collagen deposition [32]. Thirdly, to facilitate ECM remodeling, matrix metalloproteinases (MMP) are needed to degrade collagen crosslinking. MMP-2 and MMP-9 are particularly upregulated in response to mechanical loading [33]. The biological control of skin growth is, in summary, a complex process driven by local cell mechanosensing and action of cells in their immediate microenvironment.

Parallel to the interest in the underlying biological adaptation, modeling skin growth requires equally assiduous attention to this tissue's mechanical behavior. Skin is a nonlinear, transversely isotropic, and hyperelastic material that can undergo extreme deformations during tissue expansion [34, 35]. The theoretical framework to describe skin growth for finite deformations is the multiplicative decomposition of the deformation gradient into growth and elastic contributions within a continuum mechanics description [36]. This split was initially introduced to model tissue growth in response to stress by Rodriguez and coworkers just over two decades ago [37], and it was inspired by the multiplicative split of the deformation gradient used to model plasticity at finite strains [38]. The multiplicative split into growth and elastic components has been used to model the growth of tumors, the heart, blood vessels, and heart valves, to name a few examples [39–42]. An axisymmetric model of skin growth was first considered 10 years ago [43]. The growth component of the

deformation reflects the local biological adaptation. The elastic part is associated with the residual stresses induced by growth, as well as stress and deformation due to external loading. The application of this theoretical framework to predict skin growth in realistic scenarios has required the development of novel finite element methods specifically tailored to growing tissues undergoing extreme changes over time. In the case of skin, particular attention is needed to account for the mechanical behavior of this structure as a thin, nonlinear membrane [44].

The rest of this chapter is organized as follows, in the next section we cover the standard description of volumetric growth theory within continuum mechanics. Then we introduce the corresponding finite element discretization. Examples are shown next. We finish the chapter with a conclusions section.

2 Growth Theory

2.1 Kinematics

We start by introducing the reference geometry defined by material coordinates $\boldsymbol{X} \in \mathcal{B}_0$ that are mapped by φ to the current configuration $\boldsymbol{x} \in \mathcal{B}$. The local deformation is captured by the deformation gradient $\boldsymbol{F} = \partial \boldsymbol{x}/\partial \boldsymbol{X}$. The framework of volumetric growth assumes the split of the deformation gradient into growth and elastic contributions

$$\boldsymbol{F} = \boldsymbol{F}^e \cdot \boldsymbol{F}^g \tag{1}$$

Conceptually, this split involves the notion of a microscopic configuration where additional kinematic assumptions can be made [45]. Cells can change their immediate microenvironment in response to mechanical cues. These permanent changes in the local ECM define the growth component of the deformation $\boldsymbol{F}^g$. Seen in this way, the multiplicative split introduces an intermediate incompatible configuration [46]. The tensor field $\boldsymbol{F}^e$ is the local deformation required to assemble the grown differential volume elements into the current, observed, geometry. Therefore, while $\boldsymbol{F}$ is the gradient of a deformation field, neither $\boldsymbol{F}^g$ or $\boldsymbol{F}^e$ are compatible with a deformation, i.e., they are not gradients of any field. A complimentary explanation is to imagine that all we know is the current configuration and we proceed to cut this geometry into small pieces and remove all external loading. Due to residual stresses in the material, the individual pieces would deform elastically to achieve their local equilibrium or, equivalently, their stress-free state. Measuring the deformation between the stress-free state of each of these individual pieces to the current configuration would yield $\boldsymbol{F}^e$. This view of the elastic component of the deformation has led to experiments to determine the residual stresses in soft tissues. Perhaps the most well-known example of this investigation is the opening angle experiment used to determine the residual stress in arteries [47]. The residual stress field,

however, is not necessarily homogeneous over an entire tissue. In that case, a single cutting line is insufficient to reconstruct the residual stress distribution. Recent experiments on skin have characterized a non-homogeneous elastic deformation field by implementing the thought experiment described above: A sizable skin patch was cut into multiple small pieces, revealing a spatially-varying elastic deformation field induced by tissue expansion [46].

The volume change also follows the multiplicative split

$$J = J^e J^g \tag{2}$$

Where the total volume change is $J = \det(\boldsymbol{F})$, and the elastic and growth components are $J^e = \det(\boldsymbol{F}^e)$, and $J^g = \det(\boldsymbol{F}^g)$. Skin is a thin membrane and in response to stretch it grows primarily in plane. Thus, we are interested in the area change

$$\vartheta = \|\mathrm{cof}(\boldsymbol{F}) \cdot \boldsymbol{n}_0\| = \vartheta^e \vartheta^g \tag{3}$$

Which can also be decomposed into a growth term ϑ^g, and an elastic area contribution ϑ^e. The operator $\mathrm{cof}(\circ) = \det(\circ)(\circ)^T$ is the cofactor of the second order tensor $(\circ)$, and applied to the surface normal in the reference configuration $\boldsymbol{n}_0$ it yields the area change. In what follows we derive equilibrium equations in the reference configuration. We introduce the right Cauchy Green deformation tensor

$$\boldsymbol{C} = \boldsymbol{F}^T \cdot \boldsymbol{F} \tag{4}$$

However, the growth component of the deformation does not produce stress. Returning to our imaginary experiment in which we cut the current configuration into small pieces, only the elastic component of the deformation produces stress [48, 49]. The deformation tensor for the elastic component is

$$\boldsymbol{C}^e = \boldsymbol{F}^{g-T} \cdot \boldsymbol{C} \cdot \boldsymbol{F}^{g-1} \tag{5}$$

We remark that there are three main deformation measures, but only two of them are independent. In other words, the current configuration described by the deformation map φ is the observed geometry. For instance, in tissue expansion, this deformation map is a combination of both elastic deformation due to the inflation of the balloon, and permanent skin growth. Determining one of the two components of the deformation is enough to fully characterize the local kinematics. This will be important in the finite element implementation. We also note that we focus on the deformations measured with respect to the reference configuration. Alternatively, the strains could be calculated with respect to the current, deformed state [50].

2.2 Balance Equations

Mass is not conserved in growing tissues and the analysis of skin as an open thermodynamic system is required [51]. The permanent changes in volume due to the growth tensor $\boldsymbol{F}^g$ are associated with an addition of mass. Let ρ_0 denote the material density field. Since mass it is not conserved for this system, we have

$$\dot{\rho}_0 = \text{Div}(\boldsymbol{R}) + R_0 \tag{6}$$

Density can change due to a flux $\boldsymbol{R}$ or a source term R_0. The operator Div($\circ$) is the divergence operator in the reference configuration. Consequently, the mass-specific form for the balance of linear momentum balance is

$$\rho \dot{\boldsymbol{v}} = \text{Div}(\boldsymbol{F} \cdot \boldsymbol{S}) + \rho_0 \boldsymbol{b} \tag{7}$$

With $\dot{\boldsymbol{v}} = \dot{\varphi}$, $\boldsymbol{S}$ is the second Piola-Kirchhoff stress tensor, and the momentum flux is then $\boldsymbol{F} \cdot \boldsymbol{S}$. The momentum source per unit reference mass is $\boldsymbol{b}$. We remark that for open systems, the mass-specific version of the dissipation inequality contains an extra entropy source to account for the growing system, see [52] for a detailed review of the open system treatment in the context of biological growth.

2.3 Constitutive Models for Skin Growth

The multiplicative split of the deformation into growth and elastic contributions requires the definition of separate constitutive relations. The momentum flux is associated with the elastic deformation, and the biological process of mechanosensing and adaptation is linked to the growth tensor. To describe the mechanical behavior of skin we adopt a Neo-Hookean strain energy density function [53]. Other constitutive models for the elastic part are possible and have been explored. For instance, in our previous work we have also used a worm-like chain model, as well as the strain energy function proposed by Holzapfel, Ogden and Gasser, which allows consideration of skin anisotropy [54, 55]. An increasingly detailed and accurate understanding of skin mechanical behavior needs to be taken into consideration for the continuous updating of skin growth models [34]. For this chapter we restrict ourselves with the Neo-Hookean description.

The Helmholtz free energy $\psi = \widehat{\psi}(\boldsymbol{C}, \boldsymbol{F}^g)$, through the use of the dissipation inequality, yields the definition of the second Piola-Kirchhoff stress tensor as the thermodynamically conjugate tensor to the right Cauchy-Green deformation tensor

$$\boldsymbol{S} = 2\rho_0 \frac{\partial \psi}{\partial \boldsymbol{C}} = 2 \frac{\partial \psi}{\partial \boldsymbol{C}^e} : \frac{\partial \boldsymbol{C}^e}{\partial \boldsymbol{C}} = \boldsymbol{F}^{g-1} \cdot \boldsymbol{S}^e \cdot \boldsymbol{F}^{g-T} \tag{8}$$

For a classical Neo-Hookean solid the free energy takes the form

$$\rho_0 \psi = \frac{1}{2}\lambda \ln^2\left(J^e\right) + \frac{1}{2}\mu\left(\boldsymbol{C}^e : \boldsymbol{I} - 3 - 2\ln\left(J^e\right)\right) \tag{9}$$

The strain energy in (9) is parameterized by the Lame constants λ and μ. It can be further seen from (8) that the elastic deformation is the only one that produces stress, leading to the definition of elastic second Piola-Kirchhoff stress tensor

$$\boldsymbol{S}^e = 2\rho_0 \frac{\partial \psi}{\partial \boldsymbol{C}^e} = \left(\lambda \ln\left(J^e\right) - \mu\right)\boldsymbol{C}^{e-1} + \mu \boldsymbol{I} \tag{10}$$

For implementation of the finite element algorithm, the definition of the elastic constitutive moduli is also needed

$$\boldsymbol{L}^e = 2\frac{\partial \boldsymbol{S}^e}{\partial \boldsymbol{C}^e} = \lambda \boldsymbol{C}^{e-1} \otimes \boldsymbol{C}^{e-1} + \left(\mu - \lambda \ln\left(J^e\right)\right)\left[\boldsymbol{C}^e \overline{\otimes} \boldsymbol{C}^e + \boldsymbol{C}^e \underline{\otimes} \boldsymbol{C}^e\right] \tag{11}$$

For the growth component of the deformation we postulate that growth occurs primarily in plane [56, 57]. Recall that the normal to the skin surface is denoted $\boldsymbol{n}_0$, the growth tensor for area growth takes the form

$$\boldsymbol{F}^g = \sqrt{\vartheta^g}\boldsymbol{I} + \left(1 - \sqrt{\vartheta^g}\right)\boldsymbol{n}_0 \otimes \boldsymbol{n}_0 \tag{12}$$

The rate of change of the area growth, $\dot{\vartheta}^g$, is used to define the mass source in (6), $R_0 = \rho_0\left(1 + 2\sqrt{\dot{\vartheta}^g}/\sqrt{\vartheta^g}\right)$. The area growth variable is defined with a constitutive law for its rate of change. It is assumed that the rate of area growth is proportional to the elastic area strain at a point [58, 59]. This form of the growth tensor is assumed based on our knowledge of fibroblast and keratinocyte mechanosensing and experimental evidence that skin grows more in areas subjected to larger strains during tissue expansion [60, 61]. Specifically, we postulate the growth law

$$\dot{\vartheta^g} = k^g\left(\vartheta^g\right)\phi^g\left(\vartheta^e\right) \tag{13}$$

In which $k^g(\vartheta^g)$ is a weighting function to capture saturation of the growth rate at higher growth, and the function $\phi^g(\vartheta^e)$ captures the mechanosensing response and it is thus a function of the elastic area change. The weighting function is further expanded as

$$k^g\left(\vartheta^g\right) = \frac{1}{\tau}\left(\frac{\vartheta^{max} - \vartheta^g}{\vartheta^{max} - 1}\right)^{\gamma} \tag{14}$$

Where the parameter τ represents a time scale for growth, ϑ^{max} prevents unbounded growth, and γ characterizes the nonlinearity of the curve. The growth criterion is

$$\phi^g\left(\vartheta^e\right) = \left\langle \vartheta^e - \vartheta^{crit} \right\rangle \tag{15}$$

The parameter ϑ^{crit} is related to the physiological regime. In our everyday activities, skin undergoes constant deformation that may not trigger growth. Moreover, skin is naturally prestrained [14]. Therefore, growth takes place only when the elastic stretch goes beyond the physiological limits [62, 63]. The notation $\langle \circ \rangle$ is used for the Macaulay brackets.

The constitutive equations introduced in this section are clearly nonlinear, and solution of the equilibrium problem and update of the growth variable require iterative methods. The discretization and computational algorithm based on the finite element method are described in the next section. However, anticipating the need for the consistent linearization of the stress with respect to the deformation we have already introduced the elastic constitutive moduli $\boldsymbol{L}^e$. We now proceed to define the constitutive moduli with respect to the initial configuration

$$\boldsymbol{L} = 2\frac{\partial \boldsymbol{S}}{\partial \boldsymbol{C}} = \left(\boldsymbol{F}^{g-1}\overline{\otimes}\boldsymbol{F}^{g-1}\right) : \boldsymbol{L}^e : \left(\boldsymbol{F}^{g-T}\overline{\otimes}\boldsymbol{F}^{g-T}\right) + 2\left(\frac{\partial \boldsymbol{S}}{\partial \boldsymbol{F}^g} : \frac{\partial \boldsymbol{F}^g}{\partial \vartheta^g}\right) \otimes \frac{\partial \vartheta^g}{\partial \boldsymbol{C}} \tag{16}$$

The second term in (16) benefits from additional discussion. The second Piola-Kirchhoff stress is the pull-back of the elastic stress defined in the intermediate configuration. At constant total deformation $\boldsymbol{F}$, the derivative of the stress $\boldsymbol{S}$ with respect to the growth tensor consists of two terms, the derivative of the pull-back operation itself, which is clearly a function of $\boldsymbol{F}^g$, but also the derivative of $\boldsymbol{S}^e$, which can be obtained from the use of the chain rule. We have

$$\frac{\partial \boldsymbol{S}}{\partial \boldsymbol{F}^g} = -\left(\boldsymbol{F}^{g-1}\overline{\otimes}\boldsymbol{S} + \boldsymbol{S}\underline{\otimes}\boldsymbol{F}^{g-1}\right) - \left(\boldsymbol{F}^{g-1}\overline{\otimes}\boldsymbol{F}^{g-1}\right) : \tfrac{1}{2}\boldsymbol{L}^e : \left(\boldsymbol{F}^{g-T}\underline{\otimes}\boldsymbol{C}^e + \boldsymbol{C}^e\overline{\otimes}\boldsymbol{F}^{g-T}\right) \tag{17}$$

The last terms in Eq. (16) relating the growth multiplier ϑ^g to the total deformation $\boldsymbol{C}$, are computed based on the specific form of the growth tensor and the growth rate [64].

3 Finite Element Discretization

In the development of the theoretical framework in Sect. 2, all quantities of interest were presented with respect to the reference configuration. To solve the equilibrium Eq. (7) in a quasi-static approach, a finite element discretization based on a total

Lagrangian formulation is thus adopted. An alternative framework to simulate the growth of skin in tissue expansion is an Eulerian description, see [50].

In the finite element formulation, given the split of the total deformation into two contributions, each with its own set of constitutive relations, two independent variables need to be considered. Having a constitutive relation for the growth rate, we naturally choose ϑ^g as one of the independent variables. Then, considering a classical finite element methodology in the Lagrangian setting, it is straightforward to consider the total deformation as the second independent variable.

For the deformation, the degrees of freedom are given by the displacements at the nodes of the finite element mesh. We note that growth is considered as a local process, completely specified by the deformation at a point. In consequence, the growth multiplier is discretized as an internal variable at the integration points of the finite element mesh [36]. In what follows we distinguish between the solution of the local problem dictated by (13), and that of the global momentum equilibrium problem expressed in (7).

3.1 Local Problem: Growth Update

The growth update is done in each element independently. Consider the discretization of the time domain into n_{stp} subintervals

$$\mathcal{T} = \bigcup_{n=1}^{n_{stp}} [t_n, t_{n+1}] \tag{18}$$

For a given time step $[t_n, t_{n+1}]$, we are interested in calculating the update of the area growth at the end of the time step ϑ^g_{n+1}, given its value at the beginning of the time step ϑ^g_n, and the current total deformation $\boldsymbol{F}$ at t_{n+1}. The subscript $(\circ)_{t+1}$ to denote the end of the current time step will be omitted from now on. Recall that the constitutive equation for growth reported in (13) is the definition of the growth rate given the growth and elastic area changes. We adopt a backward Euler scheme to update the growth multiplier such that

$$\vartheta^g = \vartheta^g_n + \Delta t \dot{\vartheta}^g \tag{19}$$

Since this is an implicit scheme for time integration, and the growth rate is a nonlinear function of the current growth and elastic area changes, we solve for the update of the area growth using Newton-Raphson iterations. Recasting (19) into a residual $\mathrm{R}^{\vartheta} = \vartheta^g - \vartheta^g_n - \Delta t \dot{\vartheta}^g \doteq 0$, we then get the derivative needed for the local Newton iterations

$$\mathrm{K}^{\vartheta} = \frac{\partial \mathrm{R}^{\vartheta}}{\partial \vartheta^g} = 1 - \left(\frac{\partial k^g}{\partial \vartheta^g} \phi^g + \frac{k^g \partial \phi^g}{\partial \vartheta^g} \right) \Delta t \tag{20}$$

Where the functions $k^g(\vartheta^g)$ and $\phi^g(\vartheta^e)$ were defined in (14) and (15) above. Note that the growth criterion depends on the elastic area change, but the residual is constructed for the new growth multiplier under constant total deformation $\boldsymbol{F}$, i.e., constant ϑ. Therefore, Eq. (3) should be used to introduce $\vartheta^e = \vartheta/\vartheta^g$.

3.2 Global Problem: Total Deformation

We solve for the deformation of the finite element mesh to satisfy mechanical equilibrium (7). The growth of soft tissues occurs slowly in time such that inertia effects can be neglected. We thus set $\dot{\boldsymbol{v}} = 0$. We also ignore the contribution of body forces $\boldsymbol{b} = \boldsymbol{0}$. Then, consider the weak form of the mechanical equilibrium problem following integration by parts

$$\int_{\mathcal{B}_0} \nabla \delta \boldsymbol{\varphi} : (\boldsymbol{F} \cdot \boldsymbol{S})\, dV_0 = 0 \tag{21}$$

Appropriate boundary conditions should also be considered. There is no special treatment required for the boundary conditions, prescribed displacements or boundary loads can be applied in the same way as for standard finite element formulations in the finite deformation regime. In (21), the virtual displacements or test functions $\delta\varphi$ were used to transform (19) into its weak form. To discretize (19) in space we consider the partition of the domain $\mathcal{B}_0$ into n_{el} elements

$$\mathcal{B}_0 = \bigcup_{\mathrm{e}=1}^{n_{el}} \mathcal{B}_0^e \tag{22}$$

The geometry of each finite element is in turn defined by nodal positions and nodal basis functions. We apply the isoparametric Bubnov-Galerkin interpolation such that the deformation field φ^{el} and the test functions $\delta\varphi^{\mathrm{el}}$ inside of an element are interpolated with the same basis functions

$$\boldsymbol{\varphi}^{\mathrm{el}} = \sum_{i=1}^{n_{en}} N^i \boldsymbol{\varphi}_i,\ \delta\boldsymbol{\varphi}^{\mathrm{el}} = \sum_{j=1}^{n_{en}} N^j \delta\boldsymbol{\varphi}_j \tag{23}$$

Where φ_i, $\delta\varphi_j$ are the nodal values used to discretize the deformation and test function fields; N^i, N^j are the nodal shape functions, and n_{en} are the number of nodes per element. The gradients of the deformation field and the test function inside of an element follow directly from (23)

$$\nabla\boldsymbol{\varphi}^{\mathrm{el}} = \sum_{i=1}^{n_{en}} \boldsymbol{\varphi}_i \otimes \nabla N^i,\ \nabla\delta\boldsymbol{\varphi}^{\mathrm{el}} = \sum_{j=1}^{n_{en}} \delta\boldsymbol{\varphi}_j \otimes \nabla N^j \tag{24}$$

The discretized deformation and test function fields are used in the weak form of the equilibrium equation to define the global residual

$$\mathbf{R}_I^{\varphi} = \mathbf{A}_{e=1}^{n_{el}} \int_{\mathcal{B}e} \nabla N^i \cdot (\boldsymbol{F} \cdot \boldsymbol{S})\, dV_e \doteq 0 \tag{25}$$

The operator $\mathbf{A}_{e=1}^{n_{el}}$ is called the assembly operator and it links the residual associated with the node i, local to an element e, to the residual in terms of the global node numbering I. In order to find the deformation field φ that leads to the vanishing of the residual, a global Newton-Raphson iteration is needed. Note that the discretized residual (25) is highly nonlinear because of the definition of the second Piola-Kirchhoff stress in (8), compounded with the nonlinearity of the growth process. Therefore, we introduce the consistent tangent

$$\mathbf{K}_{IJ}^{\varphi} = \frac{\partial \mathbf{R}_I^{\varphi}}{\partial \varphi_J} = \mathbf{A}_{e=1}^{n_{el}} \int_{\mathcal{B}e} \left[\left(\nabla N^i \cdot \boldsymbol{F} \right)^{\text{sym}} \cdot \boldsymbol{L} \cdot \left(\boldsymbol{F}^T \cdot \nabla N^j \right)^{\text{sym}} + \nabla N^i \cdot \boldsymbol{S} \cdot \nabla N^j \boldsymbol{I} \right] dV \tag{26}$$

In summary, given the deformation φ_n and the growth ϑ_n^g at time t_n, we want to solve for the total deformation φ and the new growth ϑ^g at time t_{n+1}. To do so, an initial guess for the deformation is given $\varphi^{(0)}$. With this guess, the growth multiplier is updated at every integration point with the local Newton iterations. Then, the residual and algorithmic tangent defined in (25) and (26) are computed and used to generate the increment $\Delta\boldsymbol{\varphi} = -\mathbf{K}_{IJ}^{\varphi -1} \mathbf{R}^{\varphi}$. The deformation field then is updated $\varphi^{(1)} = \varphi^{(0)} + \Delta\varphi$. This process is iterated until convergence is achieved.

4 Examples

The above modeling framework has been used to study the fundamental mechanisms and implications of the growth process, as well as to showcase its potential for medical application [50, 65]. More recently, this theoretical framework has been paired with experiments on large animal models to get an even more in depth knowledge of the processes at the cellular scale [66]. Computational modeling of skin growth has helped us gain key insights and rationalize decision making during tissue expansion [58]. In particular, an important motivation for our work has been the lack of a gold standard for the expansion protocols [4, 67, 68]. Today, expander size and shape are chosen arbitrarily, based on the surgeons training and experience. Hence, in this section we start by presenting the simulation of skin growth for different expander geometries [54]. Ideal cases are tremendously useful to get generalizable knowledge and propose protocol guidelines. However, in clinical scenarios, every patient has a unique geometry and requires an individualized procedure. Thus, in the second portion of this section we also present the application

of our modeling framework to study skin growth in a patient-specific case of scalp reconstruction [69].

4.1 Expander Shape

Tissue expanders come in different sizes and shapes. The most common ones are spherical, crescent, rectangular and square. Anticipating the relative area growth from these different expanders has been challenging and, instead, empirical correction factors have been introduced [70]. Unfortunately, our inability to predict skin response to chronic hyper-stretch can lead to cases where not enough skin is harvested at the end of expansion and wound complications ensue [71]. In the opposite case, expansion can be aggressive and occur over a significant amount of time, resulting in excess skin that gets discarded at the time of surgery [6]. Here we present the virtual inflation of different expander shapes and show that even with the same material parameters and filled to an equal volume over the same time period, different shapes produce vastly different growth contours and overall area gain.

Figure 3 shows the finite element discretization of four different expanders. In all cases, the reference configuration was a flat, square sheet of tissue with dimensions $12 \times 12\ \text{cm}^2$, and with a thickness of 0.2 cm. A total of 1728 trilinear brick elements were used to discretize the geometry.

The material parameters used in the simulation were the Lame constants $\lambda = 0.577$ MPa, $\mu = 0.0385$ MPa. For the growth constitutive equations, the critical area strain was set to $\vartheta^{crit} = 1.01$, the maximum area growth was limited to $\vartheta^{max} = 2.4$, the timescale of growth was $\tau = 1.0$, and the nonlinearity parameter used was $\gamma = 2$. Note that the time used is non-dimensional since we are

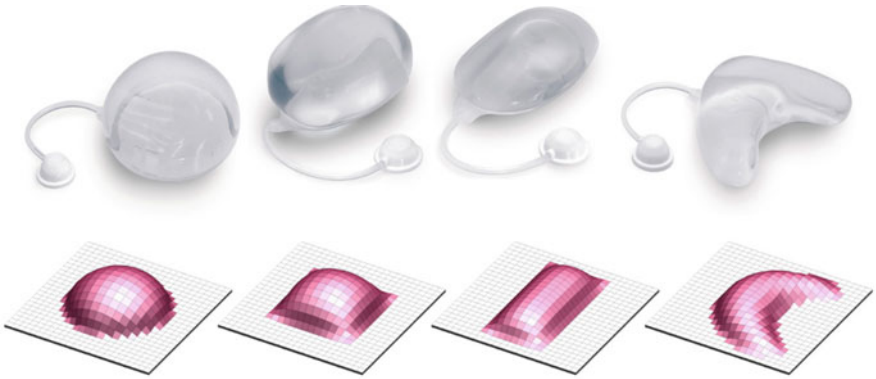

Fig. 3 Finite element modeling of different expander shapes. Four different expander shapes were simulated. The same discretization consisting of 1728 triliniear brick elements was used for all cases. The shapes depicted are, from left to right: sphere, square, rectangle, and crescent. In all cases the initial geometry was a flat sheet of tissue [53]

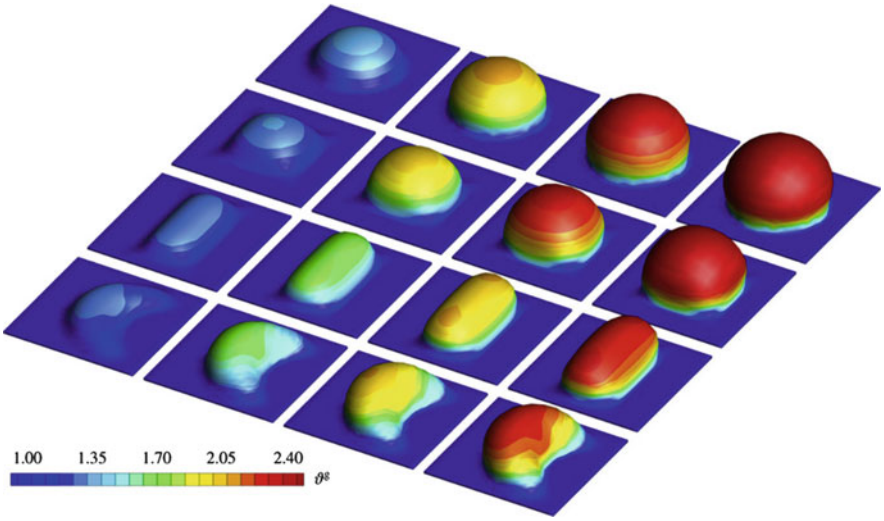

Fig. 4 Area growth due to tissue expansion. The snapshots show four consecutive time points during a virtual inflation process simulated with custom finite element tools tailored for skin growth modeling. The contours depict the amount of area growth. The apex of the expander is stretched more and also shows the greatest growth. Growth is progressively less toward the periphery of the expanded area. The same trend in the area growth distribution is seen for different expander shapes. However, total growth is different across expander geometries. The sphere expander achieves the most area gain compared to the other shapes [53]

concerned with the relative behavior across different expander shapes and not direct comparison to a clinical case.

The virtual inflation was prescribed by gradually applying a pressure of 0.002 MPa over 40 loading steps spanning a nondimensional time of $t = 4$. The skin is then left to grow under a constant pressure over the next 460 steps of $\Delta t = 0.1$ until $t = 50$. Figure 4 shows the relative area gain contours for each of the expanders over time. The area gain is calculated by measuring the total area being expanded. The initial area is measured based on the highlighted faces in Fig. 3 and is thus $A_0 = NdA$, where N is the number of faces that are part of the expanded skin and dA is the area of each face. In the beginning of the simulation all faces are square and have the same area. The final area is obtained with the sum of the growth multipliers as $A_f = \left(\sum \vartheta_e^g\right) dA$, where the subscript denotes area growth per element.

The sphere expander grows the most compared to the other expander shapes, achieving a relative area gain A_f/A_0 of 1.59, followed by the square expander which grows 1.37 in area compared to the initial state. Even though we did not calibrate the model directly to experimental or clinical evidence, this amount of growth does align with values reported in the literature. For instance, in the first tissue expansion performed by Neumann [3], an expander was filled over a span of 2 months to produce an are gain of approximately 1.5 times the initial area. The rectangular expander in our simulations grows 1.2 times in area, and the

crescent expander grows the least, achieving only 1.11 fractional area gain. These simulations underscore the importance of computational models to guide basic design principles of tissue expansion treatment. Area gain is not the only factor considered when deciding a tissue expansion protocol, but anticipating changes in area gain due to different expanders based on predictive models is a requirement for the improvement of this technique [66].

Subsequent work from our group has verified experimentally that different expanders produce different growth patterns, and that the spherical expander induces greater growth compared to the crescent expander [46]. Furthermore, we have confirmed experimentally that the growth pattern resembles the elastic and total deformation fields, with greater area growth in zones undergoing larger deformation [16]. This validates our phenomenological approach to a certain degree. Clearly, more experiments are needed to fully calibrate the computational model, especially regarding the underlying biological control, but even at the current stage, this framework is able to provide valuable and quantitative insight of how the parameters of the tissue expansion protocol are connected to the final shape and amount of newly grown skin.

4.2 Pediatric Tissue Expansion

Undoubtedly, the primary motivation for modeling skin growth in response to stretch is to transform clinical practice and improve surgery outcomes. The modeling framework presented here has been applied to study the growth of skin in patient specific geometries. In this section we present two cases of scalp reconstruction concerning the excision of a giant nevus following prolonged inflation of tissue expanders over the scalp. Reconstruction of birth defects is a common application of tissue expansion [13]. In the head and neck region, careful planning is essential but also extremely complicated [6]. In fact, currently, no predictive tool exists to aid the surgeon during preoperative planning of skin expansion. Therefore, the two cases shown here are a n important advancement towards personalized planning of tissue expansion based on computational modeling. The two inflation protocols presented are particularly interesting because a giant nevus of a similar size and location needed to be removed in both cases. Yet, despite the similarities between the two defects, different expansion protocols were performed [8, 72]. We were interested in comparing both strategies with computational modeling tools in order to assess if one alternative is more adequate than the other in terms of fractional area gain.

Starting from CT scan data, we reconstructed the skin geometry and recreated both procedures virtually with our custom finite element implementation [73]. The same material and growth parameters were used in the two cases, and the differences in growth patterns and total area growth were quantified. Figure 5 shows the photographs of the two clinical cases of interest. The top row shows a one-year old baby girl with a giant nevus in the left scalp [72]. Three tissue expanders were

Fig. 5 Tissue expansion for nevus resection. Two cases of tissue expansion are shown for two clinical cases. In the top row, the case of a one-year old baby girl is shown. Three expanders were placed, one in the forehead and two in the scalp [72]. The bottom row shows the case of a one-year old boy with a similar giant nevus. In this case, an expander was placed in the cheek, a second expander was positioned in the forehead, and a third expander was located in the top of the scalp [8]

placed, one in the forehead, one in the top of the scalp, and one in the posterior scalp. The second case is a one-year old boy with a similar giant nevus in the right scalp [8]. Three tissue expanders were used to grow the skin needed for the correction of the defect. In this case, one expander was placed in the cheek, one in the forehead, and one on the top of the scalp.

Figure 6 shows the contours of the growth multiplier for several time points of the simulation. Both cases are depicted in the same figure to allow for side-by-side comparison. For the case study I, following the clinical scenario, one virtual expander was placed in the posterior scalp. The skin in this region consisted of 2270

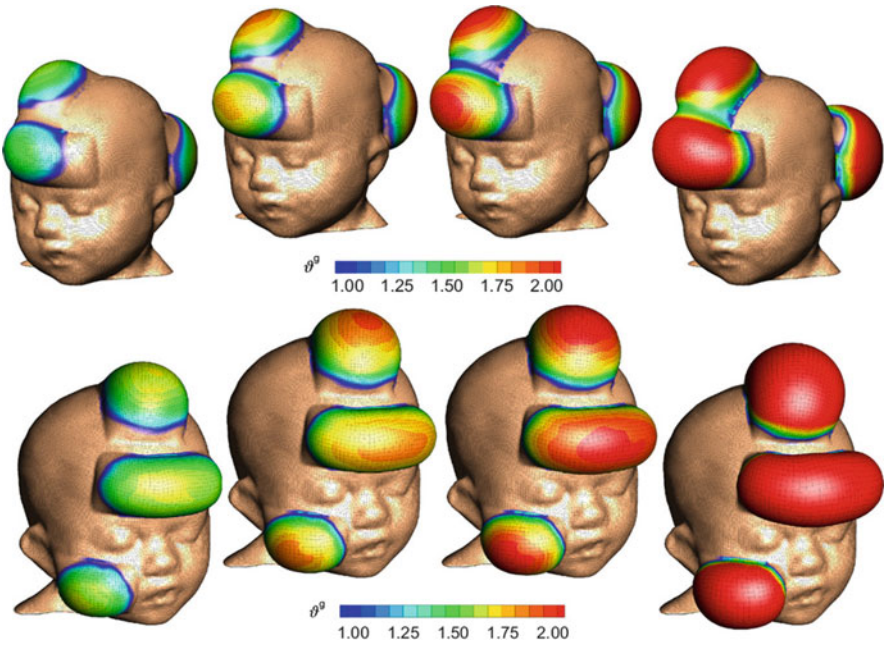

Fig. 6 Pediatric patient-specific model of tissue expansion. The top row shows the area growth contours for case I. Three expanders were placed in the forehead and scalp regions. Growth is greater at the apex of the expanded region and less toward the periphery of the expander. Area growth increases for the four time points shown. At the end of the simulation a total fractional area gain of 1.68 is achieved, and the absolute area available for reconstruction is 251.2 cm^2. The bottom row shows four snapshots for case II. A similar defect needed to be resected but in this case one expander was placed in the cheek. Area growth contours obey the same trends as seen in case I. The overall fractional area gain in this case was 1.76, however, the absolute area available for reconstruction at the end of the expansion was 227.1 cm^2. Adapted from [50] with permission

trilinear brick elements and spanned an area of 53.1 cm^2. Two more expanders were placed in the top of the scalp and the forehead. The expanded skin in this area was discretized with 3820 brick elements covering an area of 96.3 cm^2. For the case study II, aligned with the clinical case, one expander was placed in the posterior scalp, where the area of skin affected by expansion consisted of 2088 elements and covered 50.5 cm^2. An expander in the forehead and one in the cheek were then placed. The expanded forehead region was 48.8 cm^2 in area and was made up of 1800 elements. In the cheek the skin was modeled with 1200 elements and had an initial area of 29.3 cm^2.

Growth in the patient specific geometries follows the trends observed in the ideal settings of the previous section. As the expanded region is pressurized, the regions in the apex of the expander experience the greatest deformation. In consequence, skin grows more at the apex of the expander and progressively less towards the

periphery. This phenomenon is a consequence of the growth constitutive law, Eq. (13), itself based on our current understanding of skin mechanobiology.

There is always an interplay between the total, observed deformation, and the underlying tissue growth. In other words, at the beginning of the expansion process, most of the deformation is reversible, but as the process continues, skin will grow to restore the elastic stretch to ϑ^{crit}. The comparison of these two cases highlights the importance of considering patient-specific geometries when planning a procedure.

Quantitatively, for the top row of Fig. 6 corresponding to case I, the total area of expanded skin in this case starts at 149.4 cm^2, and progressively increases to 190.2 cm^2, 207.4 cm^2, 220.4 cm^2 and reaches 251.2 cm^2 by the end of the inflation process. The total fractional area gain for this case was 1.68. The different expanded regions grew differently for case I. The posterior scalp increased 1.73 in area, while the forehead and top scalp regions grew 1.66 in area. The bottom row of Fig. 6, corresponding to the case II, showed an overall fractional area gain of 1.77. The initial area of the expanded region for case II was 128.7 cm^2, and at the snapshots shown, the area increased to 176.0 cm^2, 191.3 cm^2, 202.1 cm^2 and 227.1 cm^2. Similar to case I, different expanders induced different area growth. The top of the scalp contributed 1.74 area gain, the forehead grew 1.82 the original surface, and the cheek grew by 1.72 times its initial area.

This example shows that placing the expanders in distinct anatomical regions can increase the overall area gain. At the same time, the absolute area useful for reconstruction was greater in case I. In other words, case I was not as efficient in terms of growth rate, but allowed for a greater area to be expanded and ultimately produced more skin compared to case II. We remark that the parameters used in the simulation were manually selected to match the clinical experience. A more careful calibration is needed to make more powerful predictions and impact treatment guidelines. On the other hand, these simulations were done with the same exact parameters, thus isolating the contribution of treatment strategy to area gain. This kind of insight is extremely valuable to design better tissue expansion treatments.

5 Conclusions

The future of reconstructive surgery is tied to new developments in our ability to predict skin adaptation under non-physiological regimes. Growth is one of the fundamental processes of skin tissues. Mathematical modeling of skin growth is particularly relevant in the context of tissue expansion, a reconstructive surgery technique that leverages the ability of living matter to adapt to mechanical cues [74]. Despite the popularity of this technique, we are still unable to control skin adaptation at will in order to grow skin patches of the desired area and shape. For instance, tissue expanders are the standard treatment for breast reconstruction after mastectomy, but complications and suboptimal outcomes characterized by unnatural breast shape are still common and impact cancer survivors' quality of life [68]. Tissue expansion is also widely used for reconstruction of large birth

defects such as nevus. Following skin growth, flap design is done with extreme care. However, our inability to anticipate the amount of newly grown skin and the new relaxed configuration of the skin after expander removal, can lead to excessive mechanical stress after flap closure. Tension in the flap causes delayed healing, wound dehiscence, necrosis, or hypertrophic scarring [6]. Solving these challenges relies on our ability to accurately describe skin deformation and adaptation with computational models. The progress in this area is already leading to personalized treatment and data-driven approaches in medicine [50, 54].

In this chapter we summarized the modeling framework to describe skin growth in response to supra-physiological stretch. The theoretical basis of this framework is the multiplicative split of the deformation gradient into growth and elastic contributions. This split has been adopted in the biomechanics community to model a wide variety of tissues with excellent agreement against experimental evidence [42]. Here we have specialized the general volumetric growth approach to skin tissues, characterized by area growth. The numerical solution of tissue expansion cases is achieved with custom finite element formulations [53].

In addition to modeling skin growth for its importance in tissue expansion, skin is an ideal model system to gain fundamental insight into how living tissues respond to mechanical cues. This is, at the same, a point for improvement of the current modeling approaches of finite volumetric growth: new, detailed mechanosensing models are lacking. Taking a step back, recall that the constitutive models needed to close the balance equations and fully define the problem involve two contributions. One set of constitutive relations corresponds to the elastic component of the deformation. The other constitutive law is needed for the growth component. The constitutive law for the elastic component has received significant attention over the past five decades, and many models of skin's mechanical behavior have been proposed, see [34] for a thorough and recent overview of skin mechanics. The biological aspect of growth mechanics remains poorly understood.

In this chapter we presented a phenomenological relationship connecting the elastic strain to the growth rate at one point. This simple relationship, albeit phenomenological, is indeed inspired on biological knowledge and clinical observation, and, while simple, has predicted growth patterns that were later confirmed experimentally [16, 46, 66]. However, clinical interest is turning towards therapies that control both the mechanical fields (amount and timing of expansion), as well as the cellular mechanisms implicated in skin growth due to overstretch [75]. The potential of these new techniques crucially relies on improving our understanding of how exactly the resident skin cells are sensing the mechanical cues, and how these inputs control the cell action on their local microenvironment. This remains an exciting are of research.

In terms of the computational implementation of the continuum mechanics framework, here we focused on a finite element formulation. New numerical analysis tools such as isogeometric methods are an appealing alternative to simulate skin growth. Isogeometric analysis uses basis functions that are C^1 continuous over the entire domain, enabling novel thin shell formulations for nonlinear membranes based on Kirchhoff-Love kinematics [44, 76].

Finally, in addition to sound modeling approaches and robust numerical tools, the need for extensive experimental calibration of these models cannot be understated. Work on large animal models such as the swine are currently being stablished for this purpose. Skin is advantageously exposed to the outside world and its deformation can be captured with new 3D imaging techniques that are easily incorporated into the operating room. We have used multi-view stereo to track the deformation of large porcine skin patches over long time periods. Sacrificing the animal at the end of the experiment reveals the elastic and growth components of the deformation [66]. Animal models of tissue expansion were proposed decades ago, however, they lacked a rigorous framework to distinguish the different components of the deformation [77, 78]. Our experiments have confirmed that skin grows more in the apex of the expander, and that different expander shapes induce different growth patterns. The next step in experimental calibration of the skin growth models is the acquisition of human data.

In conclusion, modeling of skin growth has advanced tremendously in the past 10 years. It is currently an exciting field with new challenges in theory, numerics, and experimentation. Addressing the gaps in the field will help us achieve personalized and predictive tools for optimal preoperative planning and improved reconstructive surgery outcomes.

References

1. Taber LA (1995) Biomechanics of growth, remodeling, and morphogenesis. Appl Mech Rev 48:487
2. Marcus J, Horan DB, Robinson JK (1990) Tissue expansion: past, present, and future. J Am Acad Dermatol 23:813–825
3. Neumann CG (1957) The expansion of an area of skin by progressive distention of a subcutaneousballoon: use of the method for securing skin for subtotal reconstruction of the ear. Plast Reconstr Surg 19:124–130
4. Manders EK, Schenden MJ, Furrey JA, Hetzler PT, Davis TS, Graham WP (1984) Soft-tissue expansion: concepts and complications. Plast Reconstr Surg 74(4):493–507
5. Bozkurt A, Groger A, O'Dey D, Vogeler F, Piatkowski A, Fuchs PC et al (2008) Retrospective analysis of tissue expansion in reconstructive burn surgery: evaluation of complication rates. Burns 34:1113–1118
6. LoGiudice J, Gosain AK (2003) Pediatric tissue expansion: indications and complications. J Craniofac Surg 14:866
7. Khalatbari B, Bakhshaeekia A (2013) Ten-year experience in face and neck unit reconstruction using tissue expanders. Burns 39:522–527
8. Gosain AK, Zochowski CG, Cortes W (2009) Refinements of tissue expansion for pediatric forehead reconstruction: a 13-year experience. Plast Reconstr Surg 124:1559–1570
9. Baker SR (1991) Fundamentals of expanded tissue. Head Neck 13:327–333
10. Pusic AL, Cordeiro PG (2003) An accelerated approach to tissue expansion for breast reconstruction: experience with intraoperative and rapid postoperative expansion in 370 reconstructions. Plast Reconstr Surg 111:1871–1875
11. Ronert MA, Hofheinz H, Manassa E, Asgarouladi H, Olbrisch RR (2004) The beginning of a new era in tissue expansion: self-filling osmotic tissue expander—four-year clinical experience. Plast Reconstr Surg 114:1025–1031

12. Schmidt SC, Logan SE, Hayden JM, Ahn ST, Mustoe TA (1991) Continuous versus conventional tissue expansion: experimental verification of a new technique. Plast Reconstr Surg 87:10–15
13. Gosain AK, Chepla KJ (2012) Giant nevus sebaceus: definition, surgical techniques, and rationale for treatment. Plast Reconstr Surg 130:296e–304e
14. Buganza Tepole A, Gart M, Purnell CA, Gosain AK, Kuhl E (2015) Multi-view stereo analysis reveals anisotropy of prestrain, deformation, and growth in living skin. Biomech Model Mechanobiol 14:1007–1019
15. De Filippo RE, Atala A (2002) Stretch and growth: the molecular and physiologic influences of tissue expansion. Plast Reconstr Surg 109:2450–2462
16. Buganza Tepole A, Gart M, Gosain AK, Kuhl E (2014) Characterization of living skin using multi-view stereo and isogeometric analysis. Acta Biomater 10:4822–4831
17. Eyckmans J, Boudou T, Yu X, Chen CS (2011) A hitchhiker's guide to mechanobiology. Dev Cell 21:35–47
18. McGrath JA, Eady RAJ, Pope FM (2004) Anatomy and organization of human skin. In: Rook's textbook of dermatology. Blackwell Science Ltd, Oxford, pp 45–128
19. Fuchs E, Raghavan S (2002) Getting under the skin of epidermal morphogenesis. Nat Rev Genet 3:199–209
20. Epstein WL, Maibach HI (1965) Cell renewal in human epidermis. Arch Dermatol 92:462
21. Lechler T, Fuchs E (2005) Asymmetric cell divisions promote stratification and differentiation of mammalian skin. Nature 437:275–280
22. Reichelt J (2007) Mechanotransduction of keratinocytes in culture and in the epidermis. Eur J Cell Biol 86:807–816
23. Margadant C, Charafeddine RA, Sonnenberg A (2010) Unique and redundant functions of integrins in the epidermis. FASEB J 24:4133–4152
24. Stupack DG, Cheresh DA (2002) Get a ligand, get a life: integrins, signaling and cell survival. J Cell Sci 115:3729–3738
25. Hertle M, Adams J, Watt F (1991) Integrin expression during human epidermal development in vivo and in vitro. Development 112:193–206
26. Runswick SK, O'Hare MJ, Jones L, Streuli CH, Garrod DR (2001) Desmosomal adhesion regulates epithelial morphogenesis and cell positioning. Nat Cell Biol 3:823–830
27. Schultz GS, Wysocki A (2009) Interactions between extracellular matrix and growth factors in wound healing. Wound Repair Regen 17:153–162
28. Kippenberger S, Bernd A, Loitsch S, Guschel M, Müller J, Bereiter-Hahn J et al (2000) Signaling of mechanical stretch in human keratinocytes via MAP kinases. J Invest Dermatol 114:408–412
29. Grinnell F (2003) Fibroblast biology in three-dimensional collagen matrices. Trends Cell Biol 13:264–269
30. Driskell RR, Lichtenberger BM, Hoste E, Kretzschmar K, Simons BD, Charalambous M et al (2013) Distinct fibroblast lineages determine dermal architecture in skin development and repair. Nature 504:277–281
31. Jiang C, Shao L, Wang Q, Dong Y (2012) Repetitive mechanical stretching modulates transforming growth factor-β induced collagen synthesis and apoptosis in human patellar tendon fibroblasts. Biochem Cell Biol 90:667–674
32. Silver FH, Siperko LM, Seehra GP (2003) Mechanobiology of force transduction in dermal tissue. Skin Res Technol 9:3–23
33. Prajapati RT, Chavally-Mis B, Herbage D, Eastwood M, Brown RA (2000) Mechanical loading regulates protease production by fibroblasts in three-dimensional collagen substrates. Wound Repair Regen 8:226–237
34. Limbert G (2017) Mathematical and computational modelling of skin biophysics: a review. Proc R Soc A Math Phys Eng Sci 473:20170257
35. Buganza Tepole A, Vaca EE, Purnell CA, Gart M, McGrath J, Kuhl E et al (2017) Quantification of strain in a porcine model of skin expansion using multi-view stereo and isogeometric kinematics. J Vis Exp 2017(122):55052

36. Himpel G, Kuhl E, Menzel A (2005) Computational modelling of isotropic multiplicative growth. Comput Model Eng Sci 8:119–134
37. Rodriguez EK, Hoger A, McCulloch AD (1994) Stress-dependent finite growth in soft elastic tissues. J Biomech 27:455–467
38. Lee EH (1969) Elastic-plastic deformation at finite strains. J Appl Mech 36(1):1–6
39. Göktepe S, Abilez OJ, Parker KK (2010) A multiscale model for eccentric and concentric cardiac growth through sarcomerogenesis. J Theor Biol 265(3):433–442
40. Roose T, Chapman SJ, Maini PK (2007) Mathematical models of avascular tumor growth. Siam Rev 49:179–208
41. Cowin SC (1996) Strain or deformation rate dependent finite growth in soft tissues. J Biomech 29:647–649
42. Ambrosi D, Ateshian GA, Arruda EM, Cowin S, Dumais J, Goriely A et al (2011) Perspectives on biological growth and remodeling. J Mech Phys Solids 59:863
43. Socci L, Pennati G, Gervaso F, Vena P (2006) An axisymmetric computational model of skin expansion and growth. Biomech Model Mechanobiol 6:177–188
44. Buganza Tepole A, Kabaria H, Bletzinger K-U, Kuhl E (2015) Isogeometric Kirchhoff-Love shell formulations for biological membranes. Comput Methods Appl Mech Eng 293:328–347
45. Cermelli P, Gurtin ME (2001) On the characterization of geometrically necessary dislocations in finite plasticity. J Mech Phys Solids 49:1539–1568
46. Buganza Tepole A, Gart M, Purnell CA, Gosain AK, Kuhl E (2016) The incompatibility of living systems: characterizing growth-induced incompatibilities in expanded skin. Ann Biomed Eng 44:1734–1752
47. Liu SQ, Fung YC (1988) Zero-stress states of arteries. J Biomech Eng 110:82–84
48. Ambrosi D, Mollica F (2002) On the mechanics of a growing tumor. Int J Eng Sci 40:1297–1316
49. Rausch MK, Kuhl E (2013) On the effect of prestrain and residual stress in thin biological membranes. J Mech Phys Solids 61:1955–1969
50. Zöllner AM, Buganza Tepole A, Kuhl E (2012) On the biomechanics and mechanobiology of growing skin. J Theor Biol 297:166–175
51. Kuhl E, Steinmann P (2003) Mass- and volume-specific views on thermodynamics for open systems. Proc R Soc A Math Phys Eng Sci 459:2547–2568
52. Kuhl E, Steinmann P (2003) On spatial and material settings of thermo-hyperelastodynamics for open systems. Acta Mech 160:179–217
53. Buganza Tepole A, Joseph Ploch C, Wong J, Gosain AK, Kuhl E (2011) Growing skin: a computational model for skin expansion in reconstructive surgery. J Mech Phys Solids 59:2177–2190
54. Buganza Tepole A, Kuhl E, Gosain AK (2012) Stretching skin: the physiological limit and beyond. Int J Non Linear Mech 47:938–949
55. Buganza Tepole A (2017) Computational systems mechanobiology of wound healing. Comput Methods Appl Mech Eng 314:46–70
56. Rivera R, LoGiudice J, Gosain AK (2005) Tissue expansion in pediatric patients. Clin Plast Surg 32:35–44
57. Chin MS, Ogawa R, Lancerotto L, Pietramaggiori G, Schomacker KT, Mathews JC et al (2010) In vivo acceleration of skin growth using a servo-controlled stretching device. Tissue Eng Part C Methods 16:397–405
58. Pamplona DC, Velloso RQ, Radwanski HN (2014) On skin expansion. J Mech Behav Biomed Mater 29:655–662
59. Austad ED, Pasyk KA, McClatchey KD, Cherry GW (1982) Histomorphologic evaluation of guinea pig skin and soft tissue after controlled tissue expansion. Plast Reconstr Surg 70:704–710
60. Erba P, Miele LF, Adini A, Ackermann M, Lamarche JM, Orgill BD et al (2011) A morphometric study of mechanotransductively induced dermal neovascularization. Plast Reconstr Surg 128:288e–299e

61. Derderian CA, Bastidas N, Lerman OZ, Bhatt KA, Lin S-E, Voss J et al (2005) Mechanical strain alters gene expression in an in vitro model of hypertrophic scarring. Ann Plast Surg 55:69–75. discussion 75
62. Flynn C, Taberner AJ, Nielsen PMF, Fels S (2013) Simulating the three-dimensional deformation of in vivo facial skin. J Mech Behav Biomed Mater 28:484–494
63. Flynn C, Taberner A, Nielsen P (2011) Mechanical characterisation of in vivo human skin using a 3D force-sensitive micro-robot and finite element analysis. Biomech Model Mechanobiol 10:27–38
64. Göktepe S, Abilez OJ, Kuhl E (2010) A generic approach towards finite growth with examples of athlete's heart, cardiac dilation, and cardiac wall thickening. J Mech Phys Solids 58:1661–1680
65. Zöllner AM, Holland MA, Honda KS, Gosain AK, Kuhl E (2013) Growth on demand: reviewing the mechanobiology of stretched skin. J Mech Behav Biomed Mater 28:495–509
66. Lee T, Vaca EE, Ledwon JK, Bae H, Topczewska JM, Turin SY et al (2018) Improving tissue expansion protocols through computational modeling. J Mech Behav Biomed Mater 82:224–234
67. Patel P a, Elhadi HM, Kitzmiller WJ, Billmire D a, Yakuboff KP (2014) Tissue expander complications in the pediatric burn patient: a 10-year follow-up. Ann Plast Surg 72:150–154
68. Cordeiro PG, McCarthy CM (2006) A single surgeon's 12-year experience with tissue expander/implant breast reconstruction: part I. A prospective analysis of early complications. Plast Reconstr Surg 118:825–831
69. Zöllner AM, Tepole AB, Gosain AK (2011) Growing skin: tissue expansion in pediatric forehead reconstruction. Biomech Model Mechanobiol 11:855–877
70. van Rappard JH, Molenaar J, van Doorn K, Sonneveld GJ, Borghouts JM (1988) Surface-area increase in tissue expansion. Plast Reconstr Surg 82:833–839
71. McCauley RL (2005) Tissue expansion reconstruction of the scalp. Semin Plast Surg 19:143–152
72. Gosain AK, Cortes W (2007) Pediatric tissue expansion for forehead reconstruction: a 13-year review and an algorithm for its use. Am Soc Plast Surg. Baltimore, Abstract 13288
73. Zöllner AM, Buganza Tepole A, Kuhl E (2012) On the biomechanics and mechanobiology of growing skin. J Theor Biol 297:166–175
74. Baker SR, Swanson NA (1990) Clinical applications of tissue expansion in head and neck surgery. Laryngoscope 100(3):313–319
75. Yang M, Li Q, Sheng L, Li H, Weng R, Zan T (2011) Bone marrow—derived mesenchymal stem cells transplantation accelerates tissue expansion by promoting skin regeneration during expansion. Ann Surg 253:202–209
76. Chen L, Nguyen-Thanh N, Nguyen-Xuan H, Rabczuk T, Bordas SPA, Limbert G (2014) Explicit finite deformation analysis of isogeometric membranes. Comput Methods Appl Mech Eng 277:104–130
77. Beauchene JG, Chambers MM, Peterson AE, Scott PG (1989) Biochemical, biomechanical, and physical changes in the skin in an experimental animal model of therapeutic tissue expansion. J Surg Res 47:507–514
78. Bartell TH, Mustoe TA (1989) Animal models of human tissue expansion. Plast Reconstr Surg 83:681–686